Fibers and Polymers 2005, Vol.6, No.3, 206-218

X-ray Diffraction Studies of Poly(aryl ether ether ketone) Fibers with Different Degrees of Crystallinity and Orientation

Ismail Karacan*

Department of Textile Engineering, Faculty of Engineering, University of Erciyes, TR-38039 Kayseri-Turkey
(Received February 16, 2005; Revised April 29, 2005; Accepted July 25, 2005)

Abstract: Structural studies of series of 'as spun' and drawn PEEK fibers have been carried out using X-ray diffraction and optical microscopy techniques. The analysis of results suggest that fibers produced at a constant draw ratio with increasing draw temperatures show enhanced orientation and crystalline behaviour. The resolved equatorial and meridional traces provide additional structural parameters in terms of crystallinity, crystallite size, and crystallite thickness. It is concluded that drawing at a temperature below T_g (i.e., 144 °C) results in poorly oriented non-crystalline materials, whereas drawing above T_g results in highly oriented semicrystalline materials. Additional drawing proved to increase the overall orientation with slight improvements in lateral order of the chain molecules. Quantitative analysis revealed that the crystallite size increases with increasing drawing temperature. The results also revealed the increased crystallite size upon additional drawing. Crystalline orientation parameter, $<P_2>_c$, suggests almost perfect orientation. In all cases, the amorphous orientation is found to be lower than the overall orientation parameter obtained from the optical birefringence. As a result of additional drawing, crystalline orientation was found to increase slightly but the increase in the orientation of non-crystalline material was found to be substantial. An average crystalline density was determined from the orthorhombic unit cell dimensions. It was found to vary as a result of processing conditions. It was also found that the value of the maximum birefringence shows heavy dependence on the chain conformation.

Keywords: Poly(aryl-ether-ether-ketone), X-ray diffraction, Drawing, Birefringence, Crystallinity, Degree of orientation

Introduction

Poly(aryl-ether-ether-ketone) was originally developed by ICI in the UK but is now commercially introduced under the trade name of Victrex® PEEK by Victrex plc of UK. PEEK is a semi-crystalline polymer melting at about 343 °C. Its limiting oxygen index is 0.42 and it has excellent resistance to solvents, acids, and alkalis. This aromatic polymer has special applications as coating and insulation material for high-performance wiring which is subject to stringent requirements in terms of flammability, heat and chemical resistance. Being thermoplastic, high molecular weight PEEK can be conveniently processed into such forms as fibers, films and mouldings. It also has an ability to bond strongly to carbon fibers when used as a matrix polymer [1-3].

Fine fibers are currently produced commercially by Xyex Ltd. in England. It has already been established that such fibers can be obtained by conventional melt spinning followed by drawing. PEEK's main applications are in the field of high performance engineering plastics, composites, and insulation coatings. Consequently, the majority of work concerned with structural characterization of PEEK has been carried out using isotropic [4-10] and oriented specimens [11-14]. The structure of oriented specimens has been reported by Dawson and Blundell [11], Yoda [12,13], and Kunugi *et al.* [14]. Rueda *et al.* [15] investigated the structure of oriented rods obtained by die drawing. Ohkoshi *et al.* [16,17] reported the structure and properties of drawn amorphous filaments of PEEK to different draw ratios at temperatures ranging from −115 °C to 300 °C. Voice *et al.* [18] reported the characterization of orientation and crystallinity of uniaxially drawn PEEK films. Lovinger and Davis [19] carried out an investigation on single crystals of PEEK and showed that the longitudinal direction of the PEEK crystal corresponds to the *b*-crystallographic axis and the molecules are normal to the lamellar plane. This phenomenon is regarded as an additional evidence for the presence of chain-folded crystallites in the PEEK structures.

The synthesis of various poly-aryl-ether-ketones is described by Attwood [20]. Recently, synthesis and properties of PEEK copolymers with pendant methyl groups are reported by Rao *et al.* [21]. Crystallization behaviour and spherulitic growth have been studied by Blundell and Osborn [4], PEEK was shown to behave in much the same way as poly(ethylene terephthalate). Blundell and Osborn [4] proposed that the semi-crystalline PEEK has a folded-chain lamellar morphology similar to other semi-crystalline polymers such as poly (ethylene terephthalate). The morphology of PEEK has been the subject of extensive studies [4,8,9,20,22]. The solution properties of PEEK have been reported, for example, by Devaux *et al.* [23]. Fratini *et al.* [24] determined crystalline structure using X-ray diffraction. The early studies on PEEK structure recognized the similarity between its structure and that of poly(p-phenylene oxide) described by Boon and Magre [25]. Liu *et al.* [26] showed the existence of polymorphism in the poly(aryl ether ketone) family of polymers.

Hay *et al.* [27] confirmed that the unit cell dimensions

*Corresponding author: ismailkaracan@erciyes.edu.tr

depend on the crystallisation temperature. They found that the unit cell dimensions decrease systematically with increasing crystallisation temperature. Similar trend was also found by Liu *et al.* [26] with the unit cell dimensions of PEEKK under different annealing temperatures. Blundell and D'Mello [28] showed using high temperature X-ray diffraction analysis that the expansion rate in the a-axis direction is three times more than that of the b-axis direction while no change in the c-axis direction was observed.

In the present investigation, series of drawn poly(aryl ether ether ketone) fibers have been studied using X-ray diffraction and optical microscopy techniques with the aim of carrying out a systematic investigation on the measurements of crystallinity, crystallite size and orientation of the crystalline and amorphous phase as well as the evaluation of crystalline density and maximum birefringence with the ultimate aim of gaining an enhanced understanding of processing-structure-property relationships.

Experimental

Materials

The as-spun PEEK fiber coded in Table 1 as S-20 with a linear density of 2.74 tex per filament was spun with a wind-up speed of 350 m/min. Samples coded as Series A listed in Table 1 were produced from S-20 at a constant nominal draw ratio of 2.42 using a heated pin set at temperatures ranging from 110 ° to 208 °C. Series B samples listed in Table 2 were produced using Sample A-4 as a starting material with draw ratios of 1.2 and 1.33, respectively. Series C samples listed in Table 3 were produced using 'as-spun' fiber spun coded as S-14 (produced with a lower wind-up speed of 102 m/min as a starting material) at a drawing temperature of 164 °C with subsequent draw ratios of 2.49

Table 1. Structural parameters of PEEK fibers (Series A): effect of drawing temperature T_d at a constant nominal draw ratio of 2.42

Sample	T_d (°C)	Δn	A_c (nm^2)	χ_c (%)	L_{co} (nm) 110	L_{co} (nm) 200	$\langle P_2\rangle_{av}$	$\langle P_2\rangle_c$	$\langle P_2\rangle_{am}$
S-20(a)	-	0.026	-	-	-	-	0.073	-	-
A-1	110	0.211	-	(39.5)	(1.8)	(0.74)	0.596	-	-
A-2	142	0.223	-	(45.9)	(3.07)	(2.05)	0.630	-	-
A-3	147	0.231	0.229	48.50	4.58	3.34	0.653	0.968	0.356
A-4	197	0.265	0.230	52.51	6.66	4.84	0.749	0.969	0.506
A-5	208	0.255	0.228	46.30	8.20	5.92	0.720	-	-

Key: (a), 'as-spun' feedstock produced at a winding speed of 350 m/min with a linear density of 2.74 tex per filament, Δn: birefringence measured at a wavelength of 550 nm, A_c: chain cross-sectional area, $\%\chi_c$: X-ray crystallinity; the values given in brackets are obtained from oriented non-crystalline peaks, L_{co}: crystallite size calculated from corrected half-height width, $\langle P_2\rangle_c$: herman's orientation parameter of the crystalline phase, $\langle P_2\rangle_{av}$: overall orientation parameter obtained from optical microscopy, $\langle P_2\rangle_{am}$: amorphous orientation parameter.

Table 2. Structural parameters of PEEK fibers (series B): effect of subsequent drawing (draw ratio λ) on the structural parameters of sample A-4

Sample	λ	Δn	A_c (nm^2)	χ_c (%)	L_{co} (nm) 110	L_{co} (nm) 200	L_{co} (nm) 002	$\langle P_2\rangle_{av}$	$\langle P_2\rangle_c$	$\langle P_2\rangle_{am}$
A-4	-	0.265	0.230	52.51	6.66	4.84	3.66	0.749	0.969	0.506
B-1	1.20	0.281	0.229	41.80	9.13	6.38	3.62	0.794	0.981	0.659
B-2	1.33	0.316	0.228	43.60	9.50	6.87	5.23	0.893	0.987	0.820

Key: see Table 1.

Table 3. Structural parameters of PEEK fibers (series C): effect of subsequent drawing on the structural parameters of sample S-14

Sample	λ	Δn	A_c (nm^2)	χ_c (%)	L_{co} (nm) 110	L_{co} (nm) 200	$\langle P_2\rangle_{av}$	$\langle P_2\rangle_c$	$\langle P_2\rangle_{am}$
S-14	-	0.011	-	-	-	-	0.031	-	-
C-1	2.49	0.198	0.228	22.5	7.20	4.54	0.559	0.969	0.440
C-2	3.66	0.290	0.227	45.9	8.77	6.25	0.819	0.983	0.680

Key: see Table 1.

and 3.66, respectively.

Birefringence Measurements

The birefringence (Δn) is defined as the difference between the two refractive indices ($n_{||} - n_{\perp}$) and is determined using equation (1)

$$\Delta n = \frac{t \cdot \lambda}{h \cdot D} \quad (1)$$

where t is the fringe shift inside the fiber, h is the interfringe spacing, λ is the wavelength of light (550 nm for white light), and D is the fiber diameter. The birefringence was measured using a Pluto polarised interference microscope equipped with a Wollaston compensator. The results presented in Tables 1-3 are an average of 5 readings with the maximum observational error of ±0.002.

X-ray Diffraction

Wide-angle X-ray diffraction patterns shown in Figure 1 were recorded on a flat plate at a sample to camera distance of 4 cm. The wide-angle X-ray diffraction traces were obtained using a modified Hilger-Watts Y115 X-ray diffractometer mounted on a Hiltonbrook DG2 constant output generator utilizing nickel filtered CuK_α radiation ($\lambda = 0.1542$ nm) and voltage and current settings of 10 kV and 30 mA, respectively. Counting was carried out at 20 steps per degree. The observed equatorial X-ray scattering data in the 10-35 ° 2θ range was corrected for polarization, Lorentz, and incoherent scatter effects and finally normalized to a convenient standard area [29].

Since the amount of polarization depends on the angle of scattering, experimentally observed array of intensities must be multiplied by the polarization factor to give polarization corrected intensity $I_2(2\theta)$:

$$I_2(2\theta) = I_1(2\theta)\frac{2}{1 + \cos^2 2\theta} \quad (2)$$

where $I_1(2\theta)$ is the array of experimental intensities as a function of diffraction angle (2θ). Lorentz scattering depends on the method of recording the intensities. The usual Lorentz factor used for normal beam single-crystal rotation was used in the present investigation. Hence polarization corrected array of intensities must be multiplied by the Lorentz factor to give Lorentz corrected intensity, $I_3(2\theta)$:

$$I_3(2\theta) = I_2(2\theta) \cdot \sin(2\theta) \quad (3)$$

Before the normalization of diffracted intensity data into electron units, incoherent scatter taking into account the number of atoms and their scattering factors is subtracted

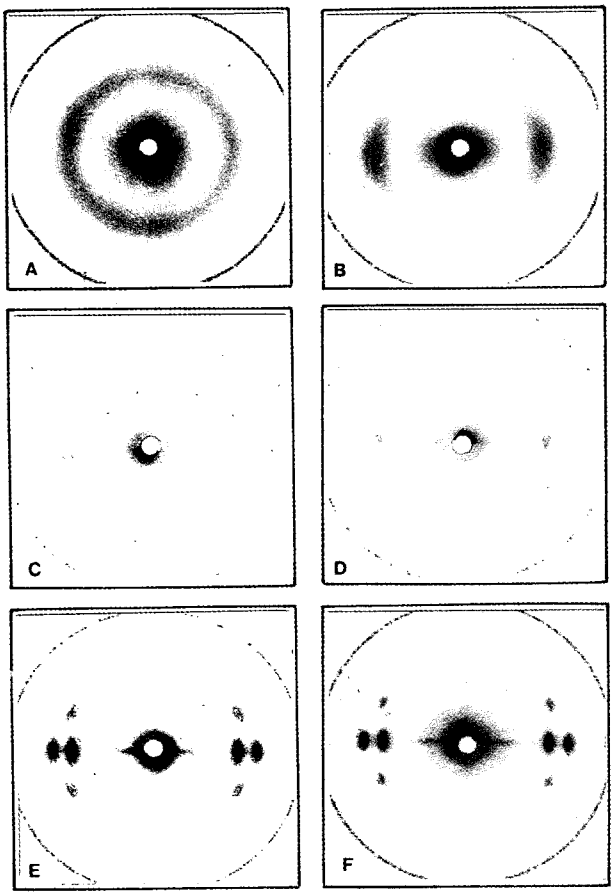

Figure 1. The WAXS patterns of PEEK fiber samples. (A) S-20, (B) A-1, (C) A-2, (D) A-3, (E) A-4, and (F) B-2. See Tables 1 and 2 for details. Fiber axes are vertical.

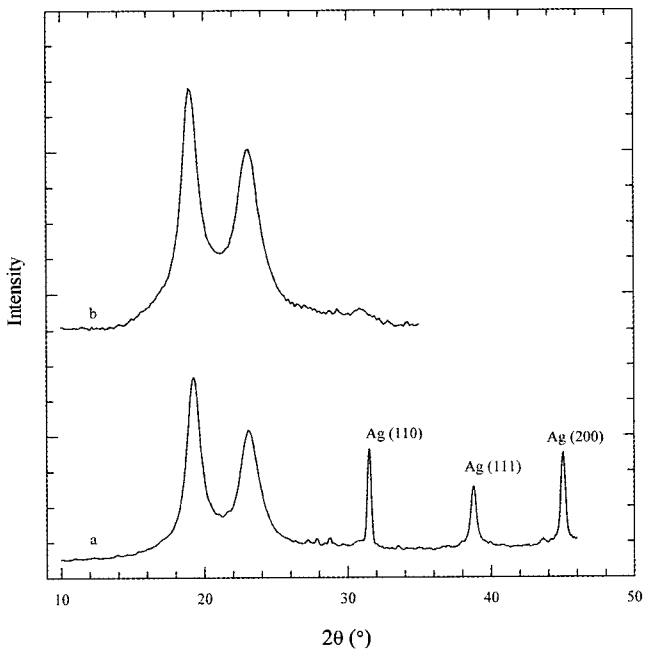

Figure 2. Calibration of X-ray diffractometer with a silver foil. (a) equatorial trace of PEEK sample with silver foil peaks, (b) equatorial trace of PEEK fiber without silver foil calibration peaks.

from the Lorentz and polarization corrected intensities as a function of diffraction angle (2θ).

A thin silver foil was used for the calibration of the 2θ positions of the diffractomer (see Figure 2). Silver foil gives three sharp peaks with d-spacings of 2.8836, 2.3523, and 2.039 Å corresponding to the (110), (111) and (200) reflections. Intensity corrected and normalized X-ray data were analysed by the peak fitting procedure detailed earlier [29] assuming a combination of Lorentzian and Gaussian line profiles (see Figures 3-5).

Following the curve fitting stages, the peak widths at half-height have been corrected using the Stoke's deconvolution procedure [30]. Hexamethylenetetramine was used for the instrumental broadening correction. Finally, the apparent crystallite size of a given reflection was evaluated using the Scherrer equation:

$$L(hkl) = \frac{K \cdot \lambda}{\beta \cdot \cos(\theta)} \quad (4)$$

where θ is the Bragg angle for the reflection concerned, λ is the wavelength of radiation (0.1542 nm), $L(hkl)$ is the mean length of the crystallite perpendicular to the planes (hkl), β is either the integral breadth or the breadth at half maximum intensity in radians and K is a Scherrer parameter.

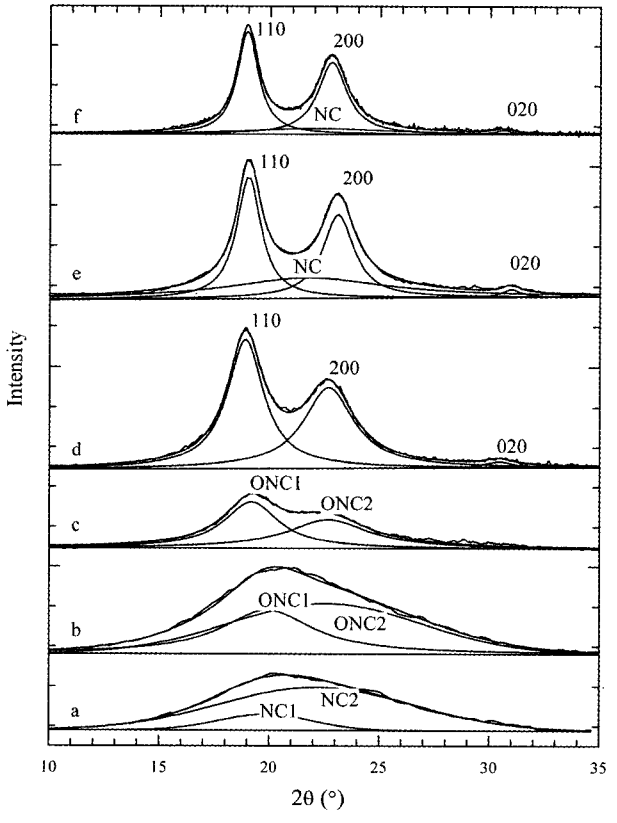

Figure 3. Resolved equatorial X-ray diffraction traces of PEEK fibers (Series A). (a) S-20, (b) A-1, (c) A-2, (d) A-3, (e) A-4, (f) A-5 (See Table 1 for details).

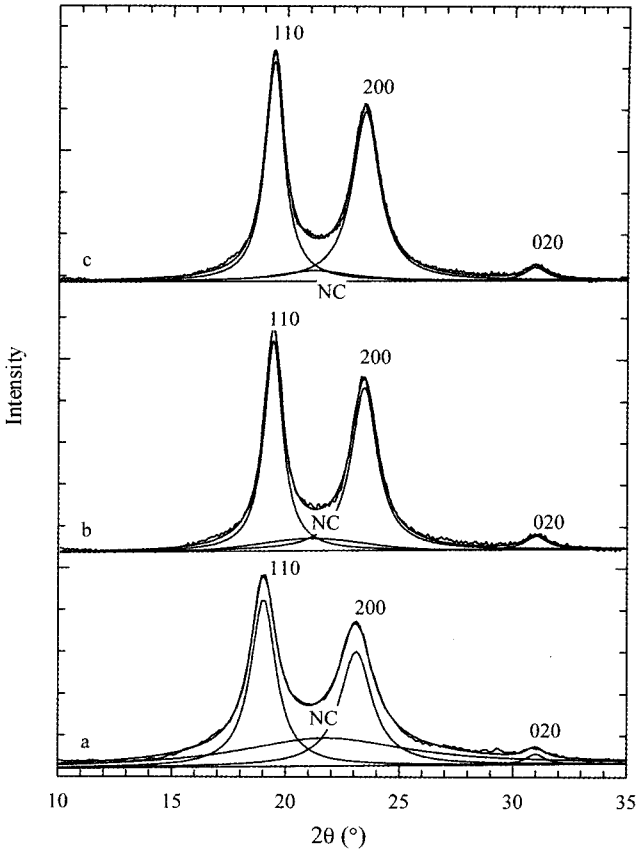

Figure 4. Resolved equatorial X-ray diffraction traces of PEEK fibers (Series B). (a) A-4, (b) B-1, (c) B-2 (See Table 2 for details).

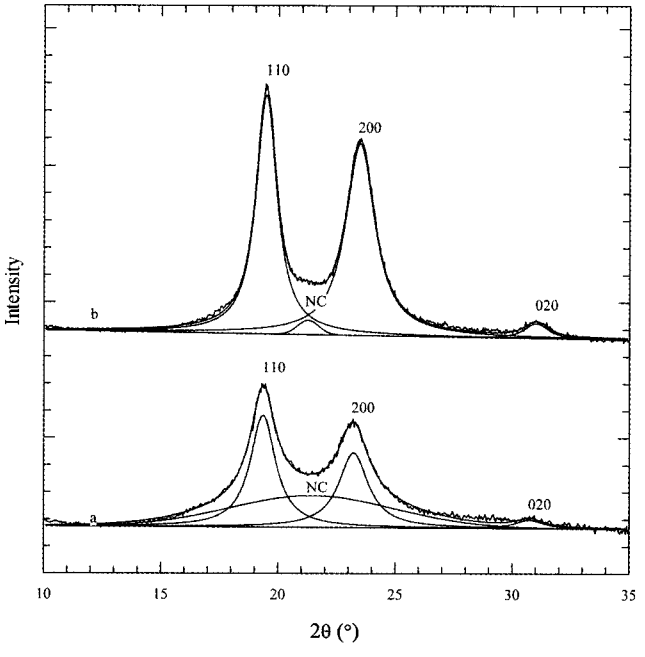

Figure 5. Resolved equatorial X-ray diffraction traces of PEEK fibers (Series C). (a) C-1, (b) C-2 (See Table 3 for details).

The azimuthal intensity profiles of the equatorial scatter were obtained by setting the counter arm at the 2θ position corresponding to the maximum peak intensity of each equatorial reflection concerned. The azimuthal intensity profile $I(\psi)$ was recorded at 0.2° intervals while the sample was rotated in a vertical plane. Data were corrected for the azimuthal broadening according to Ruland's method [31], using the width of the 002 meridional reflection as a circular broadening function parameter. Using the fiber axis as the reference direction, the orientation parameters were evaluated following the procedure described by Wilchinsky [32-34] and Karacan [35].

Data Analysis

Determination of Orientation Averages from Birefringence

The overall orientation, $\langle P_2 \rangle_{av}$, is evaluated using the birefringence (Δn) obtained from optical microscopy using equation (5);

$$\langle P_2 \rangle_{av} = \Delta n / \Delta n_{max} \tag{5}$$

where Δn_{max} is the maximum birefringence for a fully crystalline material. The results are listed in Tables 1-3.

Determination of Crystallinity from X-ray Diffraction Data

X-ray crystallinity [36] defined as the peak area crystallinity, is based on the ratio of the integrated areas of the crystalline peaks following the peak resolution to the integrated area of the total scatter under the experimental trace. This definition can be expressed as in equation (6):

$$\chi_c = \frac{\int_0^\infty I_{cr}(2\theta)d(2\theta)}{\int_0^\infty I_{tot}(2\theta)d(2\theta)} \tag{6}$$

The area under the background is considered to correspond to the non-crystalline scatter.

Determination of Crystalline Orientation Parameters from X-ray Diffraction Data

Wilchinsky [32-34] has demonstrated that the number of (hkl) planes required for obtaining $\langle \cos^2\phi \rangle$ is usually fewer than five and often only two in the case of the orthorhombic crystal systems. For PEEK fibers the value of $\langle \cos^2\phi \rangle$ was evaluated from azimuthal scans of (110) and (200) reflections, respectively. Since (200) reflection is ideal for the direct measurement of $\langle \cos^2\alpha \rangle$ for the orientation of a-crystallographic axis with respect to the c-axis, the following relationship will be valid for the present case:

$$\langle \cos^2\alpha \rangle = \langle \cos^2\phi_{200} \rangle \tag{7}$$

$\langle \cos^2\alpha \rangle$ is used for the evaluation of the orientation average of a-axis with respect to the fiber axis using equation (8):

$$F_\alpha = \frac{1}{2}(3\langle \cos^2\phi_{200} \rangle - 1) \text{ or } \frac{1}{2}(3\langle \cos^2\alpha \rangle - 1) \tag{8}$$

In the case of the b-crystallographic axis orientation, (110) reflection is used and the value of $\langle \cos^2\phi_{110} \rangle$ is evaluated by equation (9):

$$\langle \cos^2\phi_{110} \rangle = e^2\langle \cos^2\alpha \rangle + f^2\langle \cos^2\beta \rangle \tag{9}$$

where e and f are the direction cosines of the 110 plane perpendicular to the a and b-axes, respectively. Since $\langle \cos^2\alpha \rangle = \langle \cos^2\phi_{200} \rangle$, the equation (9) will lead to equation (10):

$$\langle \cos^2\beta \rangle = \frac{1}{f^2}\langle \cos^2\phi_{110} \rangle - \frac{e^2}{f^2}\langle \cos^2\phi_{200} \rangle \tag{10}$$

Using the orthogonality relationship

$$\langle \cos^2\phi \rangle = 1 - [\langle \cos^2\alpha \rangle + \langle \cos^2\beta \rangle] \tag{11}$$

The final equation for $\langle \cos^2\phi \rangle$ then becomes as follows:

$$\langle \cos^2\phi \rangle = 1 - \frac{1}{f^2}\langle \cos^2\phi_{110} \rangle + \left(\frac{e^2}{f^2} - 1\right)\langle \cos^2\phi_{200} \rangle \tag{12}$$

The values of F_ϕ, F_β and F_α for three axes are then evaluated by using equations (13-15)

$$F_\phi = \frac{1}{2}(3\langle \cos^2\phi \rangle - 1) \tag{13}$$

$$F_\beta = \frac{1}{2}(3\langle \cos^2\beta \rangle - 1) \tag{14}$$

$$F_\alpha = \frac{1}{2}(3\langle \cos^2\phi_{200} \rangle - 1) \text{ or } F_\alpha = \frac{1}{2}(3\langle \cos^2\alpha \rangle - 1) \tag{15}$$

Finally, the values of $\langle \cos^2\phi_{200} \rangle$ and $\langle \cos^2\phi_{110} \rangle$ were obtained using equations (16, 17)

$$\langle \cos^2\phi_{200} \rangle = \langle \cos^2 2\theta_{110} \rangle \langle \sin^2\psi_{200} \rangle \tag{16}$$

$$\langle \cos^2\phi_{110} \rangle = \langle \cos^2 2\theta_{110} \rangle \langle \sin^2\psi_{110} \rangle \tag{17}$$

where $2\theta_{200}$ and $2\theta_{110}$ are the Bragg angles (i.e., 2θ positions of the respective equatorial peaks obtained following the curve fitting). The values of $\sin^2\psi_{hk0}$ may be obtained by measuring the variation of intensity around the appropriate arc of the diffraction pattern. If $I(\psi_{hk0})$ is the relative intensity at angle ψ_{hk0} on the $hk0$ arc (after subtracting the background) then

$$\langle \sin^2\psi_{hk0} \rangle = \frac{\int_0^{\pi/2} I_{hk0}(\psi)\sin^2\psi_{hk0}\cos\psi_{hk0}d\psi_{hk0}}{\int_0^{\pi/2} I_{hk0}(\psi)\cos\psi_{hk0}d\psi_{hk0}} \tag{18}$$

where $I(\psi_{hk0})$ is the intensity distribution of the (110) or the (200) reflection and ψ_{hk0} is the azimuthal angle measured from the meridian (i.e., $\psi_{hk0} = 0$) to the equator (i.e., $\psi_{hk0} = 90$ °). A full description of the evaluation of $<\sin^2\psi_{hkl}>$ values is given by Stein [37] and Karacan [35].

Determination of Amorphous Orientation

Assuming a two-phase structure consisting of crystalline and amorphous material, it is possible to determine the amorphous orientation parameter, $<P_2>_{am}$, using a combination of the crystalline orientation parameter, $<P_2>_c$ obtained from X-ray diffraction analysis and the overall orientation parameter, $<P_2>_{av}$, obtained from optical microscopy using equations (19 and 20):

$$<P_2>_{av} = \chi_c<P_2>_c + (1-\chi_c)<P_2>_{am} \quad (19)$$

$$<P_2>_{am} = \frac{<P_2>_{av} - \chi_c<P_2>_c}{(1-\chi_c)} \quad (20)$$

where χ_c is the crystallinity value determined from X-ray diffraction analysis. The calculated amorphous orientation parameter, $<P_2>_{am}$, values are summarized in Tables 1-3.

Results and Discussion

Qualitative Characterization

In the first instance, the structure of the investigated fibers was assessed by inspecting wide-angle X-ray diffraction patterns shown in Figure 1. It was found that the 'as spun' fibers were non-crystalline and very poorly oriented even at the maximum winding speed of 350 m/min. A typical X-ray photograph of an 'as spun' fiber (sample S-20) is shown in Figure 1(a). Investigation of fibers (series A) produced at a constant nominal draw ratio of 2.42 using a heated pin set at temperatures ranging from 110 °C to 208 °C (see Table 1) showed that the drawing temperature substantially affects the structure of the resulting fibers (see Figure 1). As expected, the drawing resulted in increased orientation.

Fibers drawn at temperatures up to 132 °C did not show any signs of a development of three-dimensional ordered structures. In the fiber drawn at 142 °C it was just about possible to see the traces of crystalline reflections, whilst drawing at 147 °C and above resulted in the formation of oriented semicrystalline fibers. The X-ray patterns of these fibers showed that the crystallites are well oriented. However, there is also a halo with considerable azimuthal spread showing the presence of poorly oriented non-crystalline material.

From these results it is concluded that drawing carried out at temperatures above T_g (144 °C, see ref. 11) results in the formation of oriented crystallites. Further drawing of sample A-4 (drawn initially at 197 °C) using a hot plate at 275 °C (Series B, see Table 2) results in a slight improvement in the X-ray diffraction patterns.

It is well established that the maximum achievable draw ratio is influenced by the orientation of the 'as spun' fiber. For the 'as spun' fiber S-20 (birefringence; $\Delta n = 0.026$) the maximum achievable draw ratio did not exceed 3.30. Another 'as spun' fiber (S-14) produced at a lower winding speed of 102 m/min (linear density 8.22 tex), had a lower birefringence ($\Delta n = 0.011$). From this fiber it was possible to produce drawn fiber at 164 °C using a nominal draw ratio of 3.66, whilst the minimum practically achievable draw ratio at this temperature was 2.49 (series C, see Table 3). Both drawn fibers were semicrystalline; the orientation appeared to increase with increasing draw ratio.

Several attempts were made to obtain small-angle X-ray diffraction patterns. Only sample B-2 showed distinct meridional scatter with a long period of approximately 15 nm.

Quantitative Characterization

Following the qualitative characterization of the 'as-spun' and drawn fibers, a more detailed quantitative characterization has been carried in terms of the measurements of the crystallinity, crystallite size, and orientation parameters utilizing the data obtained from equatorial, meridional and azimuthal scans of the oriented PEEK fiber samples.

Equatorial traces of the samples listed in Tables 1-3 have been examined in two stages. In the First stage, a silver foil standard specimen was used with the fiber samples in order to obtain accurate peak positions (i.e., *d*-spacings) in the 10-46 ° 2θ range as shown in Figure 2(a). In the second stage, the traces were covered in the 10-35 ° 2θ range in the absence of silver foil in order to estimate the structural parameters in terms of peak area crystallinity and crystallite size (see Figure 2b). It should be noted that the silver foil was found to give a considerable contribution to the background scatter thereby relatively reducing the crystalline scatter.

Figures 3 (Series A), 4 (Series B), and 5 (Series C) show the resolved equatorial traces of the samples studied during the course of the present investigation. The obtained resolved peak parameters are presented in Table 4. In the case of series B and C, the equatorial peaks have been indexed as 110, 200, and 020, respectively.

The equatorial trace of the 'as spun' (S-20) fiber was resolved into non-crystalline peaks labeled as NC1 and NC2 with d-spacings of 0.447 nm and 0.401 nm, respectively. Due to the poor orientation with no detectable sign of three-dimensional order, the 'as-spun' fiber (S-20) contains slightly oriented amorphous material. Birefringence value of this sample ($\Delta n = 0.026$) also confirms the poor overall orientation.

As the drawing is carried out at temperatures below T_g around 110 and 142 °C, the structure starts to orient itself along the fiber axis direction as shown by the increased birefringence values together with the presence of oriented asymmetrical equatorial scatter seen in wide-angle X-ray diffraction patterns (Figures 1(B, C) and 3(b and c)). The equatorial traces of samples A-1 and A-2 shown in Figure 3 (b and c) can be resolved into oriented non-crystalline peaks

Table 4. Resolved peak parameters

Sample	Peak	*f*	*A*	*W*	*d*-obs (nm)	*A* (%)
S-20	NC1	0.99	8.00	6.00	0.447	5.6
	NC2	1.00	21.60	12.35	0.401	30.8
A-1	ONC1	1.00	43.90	5.00	0.445	14.1
	ONC2	0.00	50.45	12.23	0.394	25.4
A-2	ONC1	0.06	23.17	2.98	0.462	24.30
	ONC2	0.00	14.24	4.46	0.392	21.55
A-3	110	0.00	64.09	2.02	0.470	25.54
	200	0.12	40.20	2.76	0.392	21.25
	020	0.01	2.79	1.62	0.293	0.61
A-4	110	0.04	60.85	1.41	0.470	27.44
	NC	0.00	10.22	8.82	0.421	(24.75)
	200	0.00	26.25	1.93	0.391	23.84
	020	0.08	1.75	0.80	0.294	1.23
	002	0.34	6.80	2.50	0.488	-
A-5	110	0.01	51.70	1.16	0.469	22.76
	NC	0.00	3.35	8.00	0.422	(7.80)
	200	0.01	35.54	1.59	0.390	23.00
	020	1.00	1.88	1.00	0.293	0.51
B-1	110	0.00	52.73	1.05	0.470	20.71
	NC	1.00	2.92	6.60	0.420	(4.2)
	200	0.00	40.21	1.48	0.389	22.01
	020	0.95	2.75	1.23	0.294	0.90
	002	0.22	4.66	2.53	0.495	
B-2	110	0.02	52.26	1.01	0.469	19.76
	NC	1.0	2.57	4.00	0.419	(3.5)
	200	0.00	40.13	1.38	0.389	21.35
	020	0.34	3.02	0.72	0.294	0.72
	002	0.50	6.15	1.76	0.494	
C-1	110	0.0	24.7	1.31	0.470	12.1
	NC	0.0	7.0	9.0	0.419	(15.2)
	200	0.0	16.5	2.05	0.390	9.4
	020	0.0	1.9	1.43	0.292	1.0
C-2	110	0.0	52.44	1.09	0.467	21.1
	NC	1.0	3.10	1.27	0.419	(1)
	200	0.0	42.13	1.51	0.387	23.4
	020	0.0	3.19	0.85	0.293	1.4

Key: *f*: profile function parameter; *f* is 0 for Lorentzian and 1 for Gaussian profiles, *A*: peak height (eu), *W*: half-height width (2θ), *A*%: % peak area above the baseline.

labeled as ONC1 and ONC2 with *d*-spacings of 0.445-0.462 nm and 0.394-0.392 nm which are close to the 110 and 200 peaks observed in crystalline samples. The results show that the samples drawn below glass transition temperature of 144 °C, result in poorly oriented and disordered structures with widely separated chains and smaller crystallites. Table 4 shows the peak parameters obtained from the curve fitting of the equatorial profiles shown in Figure 3(a-c). It shows how the peak widths become narrower as the order and orientation is introduced with increasing drawing temperature. Decreasing peak width at half height is an indication of the increased crystallite size. Increasing crystallite size is also followed by an increase in the birefringence values regarded as a measure of overall orientation.

The analysis of the results shows that the molecular structure in terms of crystallinity, crystallite size and orientation improves following the drawing above glass transition temperature. The peak resolution of fibers drawn above T_g revealed three distinct crystalline peaks indexed as 110, 200, and 020, respectively (series A, B, and C). During the curve fitting stages, it was necessary to include a non-crystalline peak labelled as NC, shown in Figures 3-5, with a *d*-spacing of 0.42 nm due to a broad halo underneath the crystalline peaks to improve the fitting to an acceptable level.

A close examination of the obtained *d*-spacings of the crystalline peaks showed small differences. Thus the *d*-spacing of the 110 peak varied from 0.467 nm to 0.471 nm and the *d*-spacing of the 200 peak varied from 0.387 nm to 0.391 nm, whereas the *d*-spacing of the 020 peak varied from 0.292 nm to 0.294 nm. It is interesting to note that the cross-sectional area per chain (A_c) had no definite correlation with the drawing conditions (Tables 1-3).

The values of peak area crystallinity (i.e., X-ray crystallinity) for all the samples are given in Tables 1-3. For the samples A-1, and A-2, the X-ray crystallinity values given in brackets are best regarded to be arising from oriented non-crystalline domains present in the corresponding structures due to the relatively poor orientation, low degree of crystallinity and smaller crystallite sizes.

In Tables 1-3, the values of crystallite sizes calculated from the corrected half-height widths of the resolved profiles by applying the usual Scherrer equation are presented. It is clear that the crystallite size (L_{co}) increases as the drawing temperature is increased. The obtained results also suggest an increased crystallite size upon additional drawing. The crystallite size results summarised in Tables 1-3 obtained from the corrected half-height widths of the (110) and (200) peaks show more growth in the direction perpendicular to the 110 planes than in direction perpendicular to the 200 planes.

The meridional scans have been carried out in order to estimate the crystallite thickness by using the 002 peak profile. The results for the Series B fibers are presented in Table 2. It can be seen that the crystallite thickness does not change significantly with additional drawing. Due to the less well defined nature and weak intensity in the meridional and azimuthal direction, 002 reflection is found to be unsuitable for the direct orientation measurements. As mentioned below, strongly diffracting (110) and (200) reflections were used for

the indirect determination of orientation parameters.

Figure 6 shows the graphical representation of WAXS pattern of a typically oriented and crystalline PEEK fiber reproduced with the aid of reciprocal space lattice coordinates. The extinct reflections were not included in the graphical output in order to facilitate the comparison between the observed and the calculated reflections.

The oriented sample drawn at 197 °C with draw ratio of 1.33 has yielded the maximum number of visible reflections out to 0.25 nm. As shown in Figure 6, the total number of crystalline reflections is ten, three are equatorial, one meridional and six are seen on two layer lines. The equatorial reflections are indexed as 110, 200, and 020, whereas the main meridional reflection is indexed as 002. The off-equatorial reflections are indexed as 111, 211, 121, 102, 112, and 212, respectively.

The observed *d*-spacings are tabulated in Table 5. It should be noted that the off-equatorial reflections are determined from calibrated X-ray diffraction photographs.

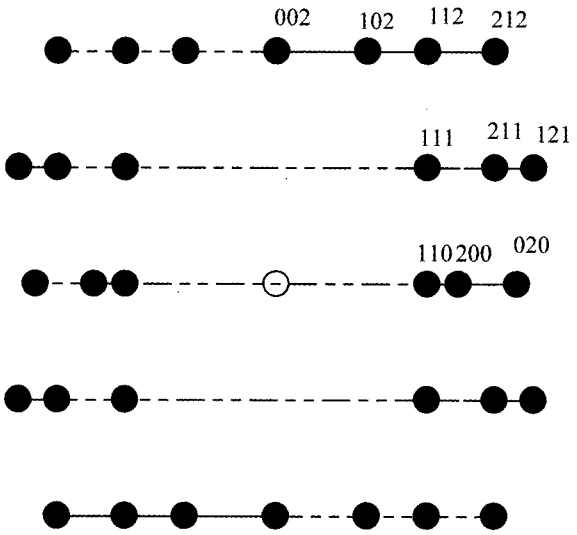

Figure 6. A graphical representation of wide-angle X-ray diffraction pattern of a highly oriented and crystalline PEEK fiber.

Table 5. Comparison of the observed and calculated *d*-spacings of sample B-2

Index	Relative intensity	*d*-obs (nm)	*d*-calc (nm)
110	s	0.470	0.470
200	s	0.389	0.389
020	w	0.295	0.295
111	s	0.421	0.424
211	s	0.306	0.308
121	w	0.267	0.265
002	w	0.495	0.495
102	m	0.415	0.418
112	m	0.337	0.341
212	w	0.267	0.272

Key: s: strong, m: medium, w: weak.

Assessment of Crystallinity Measurements

In principle, the degree of crystallinity can be defined as the relative proportion of three-dimensionally ordered structure present in a material and is usually most directly measured by wide-angle X-ray diffraction method. Apart from X-ray diffraction, it is also possible to use density, infra-red and Raman spectroscopy and thermal analysis techniques to evaluate the degree of crystallinity. Due to the sensitivity of X-ray diffraction to highly diffracting planes in semi-crystalline structures, it is usually more reliable than the other methods of measuring crystallinity. Despite the reliability of X-ray diffraction method, X-ray crystallinity may still contain small amounts of non-crystalline material, but this quantity is not expected to be very high. This kind of uncertainty is usually eliminated with the efficient use of curve fitting procedures during the separation of overlapping diffraction peaks from the disordered background. In the present study, X-ray crystallinity measurements were carried out in the 2θ range of 10 and 35 ° using equatorial diffraction profiles.

In reality, X-ray crystallinity measurements should include all the reflections in the reciprocal space including the off-equatorial and off-meridional reflections but due to the practical reasons in routine laboratory environments, only equatorial reflections are preferred. X-ray crystallinity values evaluated from equatorial scatter is best regarded as a measure of lateral order. The use of equatorial scatter simplifies the sample preparation as well. When the full reciprocal space reflections need to be used, the sample must be prepared in the form of either finely powdered form or finely chopped filaments to facilitate the collection of all the diffraction data in the reciprocal space.

X-ray crystallinity values evaluated using equation (6) are summarised in Tables 1-3. The results show an oriented non-crystalline content variation between 39.5 and 46 % for the samples (A-1 and A-2) drawn below T_g and a degree of X-ray crystallinity variation between 48.5 and 52.5 % for the samples drawn above T_g (Table 1). Additional drawing of Sample A-4 with draw ratios of 1.2 and 1.33 results in a slight reduction of crystallinity values from the starting crystallinity value of 52.5 % to 41.8-43.6 %. The slight reduction in crystallinity values are accompanied by improved crystallite sizes in the direction perpendicular to the (110) and (200) planes (Table 2). Lateral improvement is accompanied by crystallite thickness due to the thickening of the (002) planes during the additional drawing stage. Due to the highest achievable draw ratio, the highest crystallinity and crystallite size and thickness values are observed in the structure of sample B-2.

In the case of samples drawn from 'as-spun' fiber (S-14), the results suggest oriented and crystalline structures with somewhat lower X-ray crystallinity values between 22.5 and

46 % for the samples drawn with draw ratios of 2.49 and 3.66. This is believed to be due to the structure of the 'as spun' fiber drawn at a relatively low wind-up speed of 102 m/min directly affecting the molecular structure of the final drawn material.

The results confirm the importance of drawing above glass transition temperatures for the improvement of crystallinity and crystallite size values. Additional drawing is also proved to be useful for the enhancement of crystallite size and thickness. The structure of 'as-spun' fiber as a feedstock material appears to play an important role in the drawing stages.

Assessment of Orientation Measurements

Crystalline Orientation

As mentioned before, in the absence of a strongly diffracting meridional reflection, the orientation measurements of PEEK fibers were carried out using the azimuthal intensity profiles of strongly diffracting (110) and (200) equatorial reflections shown in Figure 7 utilising the azimuthal step-scan system of the diffractometer. During the curve fitting stages, it was necessary to include a peak due to the halo underneath the crystalline peaks to improve the fitting.

The azimuthal intensity traces obtained from the step-scan system were corrected for broadening according to the method developed by Ruland [31] using the half-height of the meridional (002) reflection as a circular broadening function parameter. Full details of the indirect method of measuring orientation using equatorial reflections are given by Wilchinski [32-34] and by Karacan [35]. The results are summarized in Tables 6, 7. Table 6 shows the orientational peak parameters of strongly diffracting (110) and (200) equatorial reflections of selected PEEK fiber samples obtained from the azimuthal scans in terms of profile function parameter, uncorrected and corrected half-height widths. By definition, for a pure Gaussian profile, profile function parameter is expected to approach unity. It shows that the azimuthal profiles show near Gaussian distribution. Table 7 shows the values of $<\cos^2\alpha>$, $<\cos^2\beta>$, $<\cos^2\phi>$ and the corresponding Herman's orientation parameters, F_α, F_β and F_ϕ.

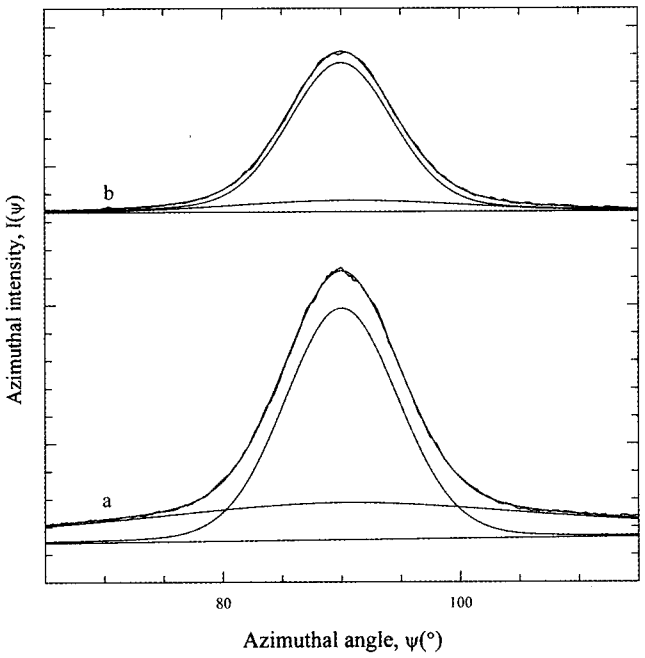

Figure 7. Resolved azimuthal intensity traces of sample (A-4). (a) (110) reflection, (b) (200) reflection.

It is noted that oriented (i.e., drawn) semicrystalline fibers of series A are already very highly oriented. Further drawing (i.e., Series B) results in a further increase in the already high crystalline orientation. It is interesting to note that in the Series B, X-ray crystallinity and orientation parameters increased only slightly, whilst the increase in birefringence was substantial. This means that further drawing results mainly in the increase of the orientation of the non-crystalline material. Results for Series C showed that increase in additional drawing

Table 6. Comparison of orientational peak parameters of various oriented PEEK fibers

Sample	Peak	f	W_{uc}(°)	W_{co}(°)
A-3	110	0.71	11.56	10.21
	200	0.75	10.75	8.54
A-4	110	0.80	11.53	10.84
	200	0.70	10.76	9.70
B-1	110	0.87	9.65	9.18
	200	0.85	8.47	7.73
B-2	110	0.94	8.88	8.40
	200	0.88	7.88	7.12
C-1	110	0.83	12.25	11.30
	200	0.76	12.33	11.04
C-2	110	0.90	9.65	9.11
	200	0.90	8.39	7.59

Key: f, profile function parameter, f: 1 for Gaussian profile, f: 0 for Lorentzian profile W_{uc}, uncorrected half-height width; W_{co}, corrected half-height width.

Table 7. Herman's orientation factors of the oriented PEEK fiber samples

Sample	$<\cos^2\alpha>$	$<\cos^2\beta>$	$<\cos^2\phi>$	F_α	F_β	F_ϕ or $<P_2>_c$
A-3	0.008	0.013	0.979	–0.488	–0.480	0.968
A-4	0.011	0.010	0.979	–0.484	–0.485	0.969
B-1	0.005	0.007	0.988	–0.492	–0.489	0.982
B-2	0.004	0.005	0.991	–0.494	–0.493	0.987
C-1	0.011	0.010	0.979	–0.483	–0.485	0.969
C-2	0.004	0.007	0.989	–0.494	–0.490	0.983

resulted in only small increase in overall orientation while the crystalline phase reached almost perfect orientation.

Amorphous Orientation

Assuming a two-phase structure consisting of amorphous and crystalline material, the amorphous phase orientation parameter, $<P_2>_{am}$, can be evaluated using equations (19 and 20) taking into account the crystallinity (χ_c) and crystalline orientation parameter, $<P_2>_c$, values obtained from X-ray diffraction analysis and the overall orientation parameter, $<P_2>_{av}$, obtained from the optical microscopy. The values of $<P_2>_{am}$ are summarized in Tables 1-3. The results show that the amorphous orientation parameter of Series A samples varies between 0.356 and 0.506, whereas the amorphous orientation parameter of sample B-2 of Series B shows remarkable improvement with an amorphous orientation parameter of 0.82 supported by the highest measured birefringence value of 0.316 in the present study. The amorphous orientation parameters of Series C samples show intermediate values as listed in Table 3. The results summarized in Tables 1-3 and in Figure 8 show that the crystalline orientation parameter, $<P_2>_c$, is, as expected, higher than the overall orientation parameter, $<P_2>_{av}$, which is in turn higher than the amorphous orientation parameter, $<P_2>_{av}$.

Unit Cell Dimensions and Re-Constructed Chain Conformation

The coordinates of the single chain shown in Figure 9 have been re-calculated using the standard bond lengths and

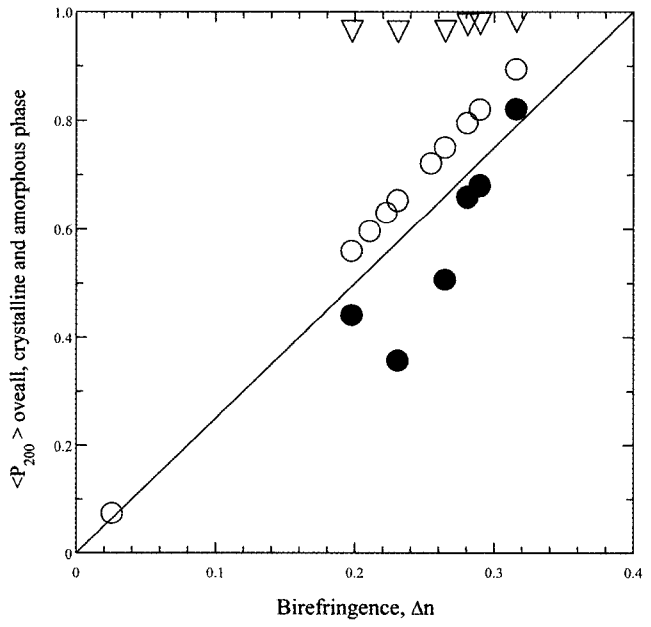

Figure 8. Comparison of birefringe (Δn) with $<P_{200}>$ values of overall, crystalline and amorphous phase. (▽) crystalline orientation, (○) overall orientation $<P_{200}>$ from birefringence, (●) amorphous orientation.

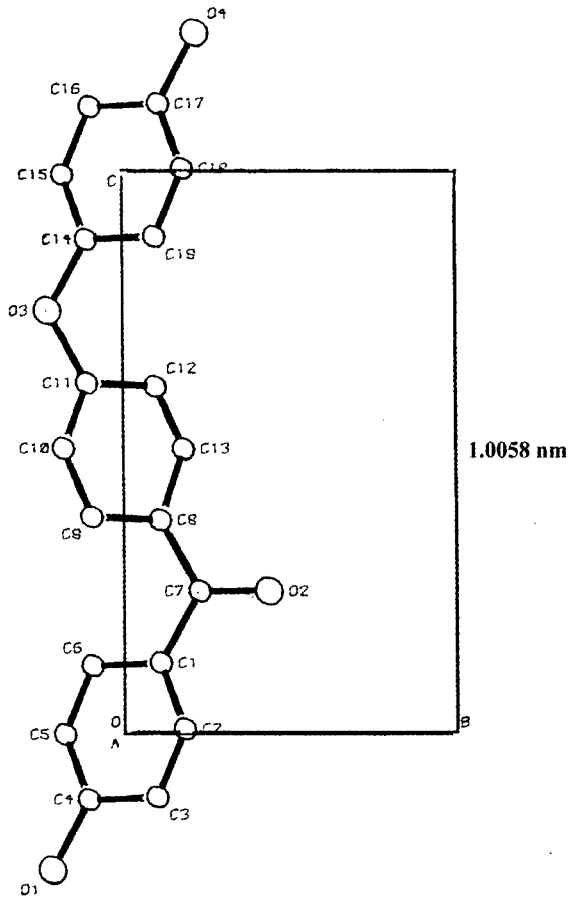

Figure 9. Atom numbering scheme of carbon atoms for the three-ring repeat unit. Hydrogen atoms are not included for the sake of simplicity. Projection on the *b-c* plane.

angles (see Table 9) of Hummel and Flory [46]. The main chain angle between the adjacent phenylene rings is taken as 124.6° as suggested by Hay *et al.* [5]. The rotation angle of the phenylene groups round the O-O or O-(C=O) axis is taken as ±40° as published in the literature [5]. This angle is denoted by Φ in the present study. The angle Φ is assumed to be zero when the plane of the phenylene group is perpendicular to the (100) plane. The same atomic coordinates were used for the determination of maximum birefringence discussed below.

As can be seen from the published data, there are some discrepancies between the unit cell dimensions (see Table 8). This is particularly true for the *c*-value, which is considerably less than the calculated values. In this study, *c*-values are found to vary between 0.977 and 0.991 nm (Table 8) within the precision of the experimental conditions compared with the calculated value of 1.0058 nm (see Figure 9). Dawson and Blundell [11] reported the *c*-value of PEEK as 1.0 nm, Hay *et al.* [5] as (1.056± 0.014) nm, and Rueda *et al.* [15] as (0.9883 ± 0.0005) nm. It is clear that these variations will inevitably lead to differences in the crystallographic volume of the unit cell and crystalline density.

Table 8. Comparison of the unit cell parameters of PEEK obtained by various investigators

Ref.	*a* (nm)	*b* (nm)	*c* (nm)	ρ_c (g/cm^3)
Rueda *et al.* [15]	0.775	0.589	0.9883	1.415
Dawson and Blundell [11]	0.775	0.586	1.000	1.400
Blundell and Newton [47]	0.776	0.589	0.995	1.404
Wakelyn [6]	0.788	0.594	1.016	1.341
Hay *et al.* [5]	0.778	0.592	1.056	1.378
Fratini *et al.* [24]	0.783	0.594	0.986	1.392
Kumar *et al.* [9]	0.779	0.591	1.000	1.384
Voice *et al.* [18]	0.797	0.593	0.980	1.380
Shimizu *et al.* [39]	0.780	0.592	1.000	1.382
Abraham and Haworth [42]	0.780	0.590	-	-
Sample A-4	0.783	0.588	0.977	1.417
Sample B-1	0.779	0.588	0.987	1.409
Sample B-2	0.778	0.589	0.991	1.405
Sample C-2	0.774	0.586	-	-

During the course of this study, the position of the meridional peak (002) has been employed to establish the *c*-axis dimension of the corresponding unit cell. Dawson and Blundell [11] argue that the *c*-value of PEEK arises not from the chemical repeat unit but from a fully extended planar subunit of two phenylene rings joined either by an ether and a ketone or two ether links.

It is worth pointing out that the broadening of the 002 peak may be attributed to the irregular stacking of the ether or ketone linking groups. The unit cell of the PEEK specimen is orthorhombic with cell dimensions as shown in Table 8. The volume of the unit cell calculated from the cell dimensions obtained in this work varies from 0.450 to 0.454 nm^3.

The corresponding calculated crystalline density values vary from 1.405 to 1.417 g/cm^3 with an average crystalline density of 1.410 ± 0.005 g/cm^3 being in good agreement with the reported values (see Table 8). In particular, Wakelin [41] reported the variation of the crystalline density between 1.367 for crystals obtained at the lowest annealing temperature of 189 °C and to 1.41 g/cm^3 for those crystals obtained at the highest annealing temperature of 323 °C. Liu *et al.* [40] also reported similar findings for the unit cell dimensions of PEEKK.

Determination of Maximum Birefringence

The principal chain polarizabalities of PEEK were calculated using the chain conformation described above together with the values of bond polarizabilities given by Bunn [43] (see Table 10).

The chain anisotropy can be calculated using the bond polarizabilities and the angles between different bonds [43-45]. Chain polarizabilities in three directions (*a*, *b*, and *c*) are given by the following equations:

$$\alpha_a = \sum[(\alpha_{||} - \alpha_{\perp})\sin^2\theta\cos^2\phi + \alpha_2] \quad (21)$$

$$\alpha_b = \sum[(\alpha_{||} - \alpha_{\perp})\sin^2\theta\sin^2\phi + \alpha_2] \quad (22)$$

$$\alpha_c = \sum[(\alpha_{||} - \alpha_{\perp})\cos^2\theta + \alpha_2] \quad (23)$$

where the summation is over the whole chemical repeat unit, θ is the angle between the bond and the *c*-axis, and ϕ is the angle where the projection of the bond in the *a*-*b* plane makes with the *a*-axis. $\alpha_{||}$ and $\alpha_{\perp}$ are the bond polarizabilities parallel and perpendicular to the bond, respectively (see Table 10).

Using the re-calculated atomic coordinates mentioned above, the chain polarizabilities in three directions are calculated to be as:

$\alpha_a = 2.40 \times 10^{-23}$ cm^3

$\alpha_b = 3.18 \times 10^{-23}$ cm^3

$\alpha_c = 3.95 \times 10^{-23}$ cm^3

The required values of refractive indices in three directions (i.e., n_a, n_b, n_c) and birefringence (Δn) can be calculated by

Table 9. Bond lengths and angles according to Hummel and Flory [46]. C_{ar} and C(O) denotes aromatic and carbonyl carbons, respectively

Bond	Length (nm)
$C_{ar} - C_{ar}$	0.139
$C_{ar} - C(O)$	0.149
$C(O) - O$	0.137
$C_{ar} - O$	0.141
$C(O) = O$	0.123

Bonds	Angle (°)
$C_{ar} - C_{ar} - C_{ar}$	120.0
$C_{ar} - C_{ar} - X$	120.0
$C_{ar} - C(O) = O$	123.0
$C_{ar} - C(O) - O$	110.9
$C(O) - O - C_{ar}$	118.3

X denotes any atom.

Table 10. Bond polarizabilities of various bonds according to Bunn [43]

Bond	$\alpha_{||} \times 10^{-25}$ cm^3	$\alpha_{\perp} \times 10^{-25}$ cm^3
$C_{ar} - C_{ar}$	22.5	4.8
$C_{ar} - C_{ali}$	14.0	3.0
C – H	8.2	6.0
C – O	14.6	1.7
C = O	20.0	10.0

substituting the chain polarizability values listed above into the Lorentz-Lorenz expression in equation (24):

$$\frac{(n^2-1)M}{(n^2+2)\rho} = \frac{4\pi}{3}\alpha N \quad (24)$$

where n is the appropriate refractive index, M is the molecular weight of repeat unit (288 daltons), ρ is the density of the material, N is the Avagadro number (6.0226×10^{23} mole^{-1}), and α is the polarizability of the whole repeat unit of a polymer chain. Using a PEEK crystalline density of 1.410 ± 0.005 g/cm^3 determined from the X-ray diffraction analysis of the present investigation and the above values of chain polarizabilities in three directions, refractive indices in three directions, n_a, n_b, and n_c, were calculated as 1.505, 1.715, and 1.964, respectively. The birefringence of a fully crystalline perfectly oriented fiber is approximated by equation (25) and for the above refractive indices its value is 0.354:

$$\Delta n = n_c - \frac{n_a + n_b}{2} \quad (25)$$

It is clear that the above calculations do not consider the effects of an internal field arising from neighbouring bonds within the chain molecule or neighbouring chain molecules in a crystal. Any consideration for such effects is bound to lower the maximum birefringence. Using the same values of bond polarizabilities, Kumar *et al.* [9] calculated the birefringence of single PEEK chain as 0.345. They arrive at values of 2.31×10^{-23}, 3.38×10^{-23}, and 4.02×10^{-23} cm^3, respectively, for the chain polarizabilities in three directions. These values correspond to refractive indices of 1.48, 1.77, and 1.97 in three directions, respectively. Voice *et al.* [18] using the atomic coordinates of Fratini *et al.* [24] containing the ring rotation angle of $\pm 37°$ and the bond polarisabilities of Bunn [43] arrived at a maximum birefringence of 0.302. Shimuzi *et al.* [39], again, using the phenyl rotation angle of $\pm 37°$ and the bond polarizabilities of Bunn [43] obtained a maximum birefringence value of 0.321. Yet, these maximum birefringence values are very close to the experimental birefringence value of 0.316 measured for the sample B-2 in the present sample. Table 11 shows the list of calculated refractive indices and birefringence values published in the literature. The differences between the calculated values are clearly dependent on the atomic coordinates and the internal phenyl ring rotation angles.

Table 11. Comparison of the refractive indices and maximum birefringence of PEEK evaluated by various investigators

Ref	n_a	n_b	n_c	Δn
Kumar *et al.* [9]	1.48	1.77	1.97	0.345
Voice *et al.* [18]	1.514	1.729	1.924	0.302
Cakmak [38]	1.5247	1.7450	1.9448	0.310
Shimizu *et al.* [39]	1.507	1.732	1.936	0.321
This work	1.505	1.715	1.964	0.354

In the present study, highly oriented PEEK fibers give observed birefringence values of up to 0.316. The discrepancy between the observed and the calculated values may be attributed to the presence of less perfect orientation in the fibers and the presence of amorphous regions as well as form birefringence which results from the anisotropic shape of the crystallites or voids embedded in a matrix with different refractive indices.

Conclusions

A systematic structural characterization of a series of oriented PEEK fibers has been carried out using wide-angle X-ray diffraction and optical microscopy techniques. Qualitative analysis of X-ray diffraction patterns of fibers produced at a constant nominal draw ratio of 2.42 at draw temperatures ranging from 110° to 208°C showed the substantial effects of drawing temperature on the structure of the resulting fibers in terms of enhanced orientation and crystallinity.

Fibers drawn at temperatures above glass temperature of 144°C resulted in the formation of oriented semicrystalline fibers. The X-ray patterns of these fibers showed that the crystallites are well oriented with a presence of a halo with considerable azimuthal spread showing the presence of poorly oriented non-crystalline material. In all cases, additional drawing resulted in enhanced orientation, crystallinity and crystallite size. Crystallite size in the direction perpendicular to the 110 planes is grown more than in the direction perpendicular to the 200 planes. Crystallite thickness showed no significant improvement with additional drawing.

Quantitative analysis revealed that the crystallite size (L_{co}) evaluated from the corrected half-height widths of strongly diffracting (110) and (200) reflections increases with increasing drawing temperature. The results also revealed the increased crystallite size upon additional drawing.

Crystalline orientation parameter, $\langle P_2 \rangle_c$, obtained indirectly from the azimuthal intensity profiles of strongly diffracting (110) and (200) equatorial reflections, suggests almost perfect orientation showing variation between 0.97 and 0.99 with corresponding chain orientation angle variation of 8.4° and 5.4°, respectively.

The amorphous phase orientation parameter, $\langle P_2 \rangle_{am}$, evaluated from a combination of crystalline orientation parameter, $\langle P_2 \rangle_c$, obtained from X-ray diffraction analysis and overall orientation parameter, $\langle P_2 \rangle_{av}$, obtained from optical microscopy shows substantial improvement with additional drawing. In all cases, as expected, the amorphous orientation parameter is found to be lower than the overall orientation parameter.

Crystalline density was evaluated using the orthorhombic unit cell dimensions. It was found to change as a result of processing conditions. It was also found that the value of maximum birefringence is heavily dependent on the chain conformation.

Acknowledgements

The author would like to thank Ken Arnold of School of Design (former Department of Textile Industries) of Leeds University, England for the supply of the samples investigated in the present study. Special thanks go to an anonymous reviewer for making very valuable and useful comments.

References

1. P. J. Hine, B. Brew, R. A. Ducket, and I. M. Ward, *Comp. Sci. Tech.*, **40**, 47 (1991).
2. C. C. Jeng and M. Chen, *Comp. Sci. Tech.*, **60**, 1863 (2000).
3. P. Werner, V. Altstadt, R. Jaskulka, O. Jacobs, J. K. Sandler, M. S. P. Shaffer, and A. H. Windle, *Wear*, **257**, 1006 (2004).
4. D. J. Blundell and B. N. Osborn, *Polymer*, **24**, 953 (1983).
5. J. N. Hay, D. J. Kemmish, J. I. Langford, and I. M. Rae, *Polymer (Commun.)*, **25**, 175 (1984).
6. N. T. Wakelyn, *Polymer (Commun.)*, **25**, 306 (1984).
7. J. N. Clark, F. G. Herring, and N. R. Jagannathan, *Polymer (Commun.)*, **26**, 329 (1985).
8. R. H. Olley, D. C. Bassett, and D. J. Blundell, *Polymer*, **27**, 344 (1986).
9. S. Kumar, D. P. Anderson, and W. W. Adams, *Polymer*, **27**, 329 (1986).
10. T. Susaga and M. Hagiwara, *Polymer*, **27**, 821 (1986).
11. P. C. Dawson and D. J. Blundell, *Polymer*, **21**, 577 (1980).
12. O. Yoda, *Polymer (Commun.)*, **25**, 238 (1984).
13. O. Yoda, *Polymer (Commun.)*, **26**, 16 (1985).
14. T. Kunugi, A. Mizushima, and T. Hayakawa, *Polymer (Commun.)*, **27**, 175 (1986).
15. D. R. Rueda, F. Ania, A. Richardson, I. M. Ward, and F. J. B. Calleja, *Polymer (Commun.)*, **24**, 258 (1983).
16. Y. Ohkoshi, H. Ohshima, T. Matsuhisa, K. Toriumi, and A. Kondo, *Sen-i Gakkaishi*, **45**, 509 (1989).
17. Y. Ohkoshi, H. Ohshima, T. Matsuhisa, K. Toriumi, and A. Kondo, *Sen-i Gakkaishi*, **46**, 87 (1990).
18. A. M. Voice, D. I. Bower, and I. M. Ward, *Polymer*, **34**, 1154 (1993).
19. A. J. Lovinger and D. Davis, *Polymer (Commun.)*, **26**, 322 (1985).
20. T. E. Attwood, P. C. Dawson, J. L. Freeman, L. R. J. Hoy, J. B. Rose, and P. A. Staniland, *Polymer*, **22**, 1096 (1981).
21. V. L. Rao, P. U. Sabeena, A. Saxena, C. Gopalakrishnan, K. Krishnan, P. V. Ravindran, and K. N. Ninan, *Eur. Poly. J.*, **40**, 2645 (2004).
22. F. J. Medellin-Rodriguez and P. J. Phillips, *Polym. Eng. Sci.*, **30**, 860 (1990).
23. J. Devaux, D. Delimoy, D. Daoust, R. Legras, J. P. Mercier, C. Strazielle, and E. Nield, *Polymer*, **26**, 1994 (1985).
24. A. V. Fratini, E. M. Cross, R. B. Whitaker, and W. W. Adams, *Polymer*, **27**, 861 (1986).
25. J. Boon and E. P. Magre, *Die Makromolekulare Chemie*, **126**, 130 (1969).
26. T. Liu, S. Wang, Z. Mo, and H. Zhang, *J. Appl. Poly. Sci.*, **73**, 237 (1999).
27. J. N. Hay, J. I. Langford, and J. R. Lloyd, *Polymer*, **30**, 489 (1989).
28. D. J. Blundell and J. D'Mello, *Polymer*, **32**, 304 (1991).
29. A. M. Hindeleh, D. J. Johnson, and P. E. Montague in "Fibre Diffraction Methods", (A. D. French and K. H. Gardner Eds.), p.149, ACS Symp. No. 141, American Chemical Society, Washington DC, 1983.
30. A. R. Stokes, *Proc. Phys. Soc.*, **A166**, 283 (1948).
31. W. Ruland, *J. Appl. Phys.*, **38**, 3585 (1967).
32. Z. W. Wilchinski, *J. Appl. Phys.*, **30**, 792 (1959).
33. Z. W. Wilchinski, *J. Appl. Phys.*, **31**, 1969 (1960).
34. Z. W. Wilchinski, *Advances in X-ray Analysis*, **6**, 231 (1962).
35. I. Karacan, Ph.D Thesis, University of Leeds, 1986.
36. A. M. Hindeleh and D. J. Johnson, *Polymer*, **19**, 27 (1978).
37. R. S. Stein, *J. Polym. Sci.*, **31**, 327 (1958).
38. M. Cakmak, *J. Polym. Sci. Polym. Lett.*, **27**, 119 (1989).
39. J. Shimizu, T. Kikutani, Y. Ookoshi, and A. Takaku, *Sen-i Gakkaishi*, **41**(11), 59 (1985).
40. T. Liu, Z. Mo, H. Zhang, H. Na, and Z. Wu, *Eur. Polym. J.* **33**, 913 (1997).
41. N. T. Wakelyn, *J. Polym. Sci., Polym. Lett. Ed.*, **25**, 25 (1987).
42. R. J. Abraham and I. S. Haworth, *Polymer*, **32**, 121 (1991).
43. C. W. Bunn, "Chemical Crystallography", p.312, Oxford University Press, London, 1961.
44. J. Furukawa, S. Yamashita, T. Kotani, and M. J. Kawashima, *J. Appl. Polym. Sci.*, **13**, 2527 (1969).
45. E. J. Roch, R. S. Stein, and E. L. Thomas, *J. Polym. Sci., Polym. Phys. Ed.*, **18**, 1145 (1980).
46. J. P. Hummel and P. J. Flory, *Macromolecules*, **13**, 484 (1980).
47. D. J. Blundell and A. B. Newton, *Polymer*, **32**, 308 (1991).